An Experimental and Theoretical Analysis of Surface Generation in Ultra-precision Grinding of Hard and Brittle Materials

CHEN Shanshan[1,2*], Cheung Chi Fai [2], ZHANG Feihu[1]

1 *School of Mechatronics Engineering, Harbin Institute of Technology, Harbin 150001, China*
2 Partner State Key Laboratory of Ultraprecision Machining Technology, Department of Industrial and Systems Engineering, The Hong Kong Polytechnic University, Hung Hom, Kowloon, Hong Kong
*Corresponding author: shanshan.chen@connect.polyu.hk Fax: (852)23625267

Abstract: This paper presents an experimental and theoretical study of surface generation in ultra-precision grinding of hard and brittle materials. The study takes into account material properties, the relative vibration between the grinding wheel and the workpiece, machining parameters and the phase shift of the grinding process. The Taguchi approach is employed to study the influence of machining parameters on the surface quality and shows the feed speed and rotational speed of the workpiece are key factors. Experiments have been conducted to study individual variable and the results further show that the feed rate and the cross-feed distance have significant effect on the surface generation. It is found that the spirals around the central area of the workpiece are the primary mechanism for surface generation, which originates from the synchronous relative tool-work vibration. The integral part of the ratio of the rotational speed of the grinding wheel to rotational speed of the workpiece determines the number of the spirals and its fractional part controls the spiral geometry. A theoretical model for predicting the single spiral generation has been developed to explain the accumulation of the phase shift and the geometry. The changeable feed speed near the end of grinding is also modelled, revealing the approximate straight lines around one circle in the central region. The simulated results indicate the theoretical models and the ground surfaces are in close agreement. The scallop-height model is developed to calculate the influence of phase shift on surface quality and it is found that the phase shift near the medium value can effectively improve surface quality. Finally, a comparison for different surface generation mechanisms in grinding mould Steel, tungsten carbide (WC) and reaction bonded silicon carbide (RB-SiC) is investigated. It is interesting to note that the Spanzipfel effect contributes to the surface generation not only on ductile materials such as mould Steel but also on brittle materials such as WC and RB-SiC. The Spanzipfel effect is most significant in grinding mould Steel. For WC and RB-SiC, the ground surface contains both ductile region and brittle region in form of micro fracture.

Key words: Spiral; phase shift; Spanzipfel; surface generation mechanism; ultra-precision grinding; hard and brittle materials.

1. Introduction

Ultra-precision grinding is widely applied to machine hard and brittle materials with high surface integrity and low surface roughness [1-4]. The reaction bonded silicon carbide (RB-SiC) ceramic has become the preferred mirror material for space telescopes due to its excellent mechanical properties, such as high hardness, high rigidity and chemical inertness [5-7]. However, it is a challenge to obtain a desirable surface finish in the grinding due to its low fracture toughness. Surface quality is the crucial indicator to evaluate the grinding performance, which results from the interaction of the tool and machined material. A high-quality surface finish significantly improves the functional performance of components, such as fatigue strength, frictional properties and part life [8, 9]. Surface generation, as an important issue in the grinding process, is directly related to the surface quality and functional performance of the workpiece. This has attracted much research attention due to the ever-increasing requirements of precision components with good surface finish. However, the surface generation in ultra-precision grinding is affected by multiplicity of variables involving the wheel geometry, abrasive distribution, material properties and grinding operation conditions. This is particularly true for the random nature of the cutting edges on the wheel which makes it difficult to study the process of surface generation and surface topography as compared with deterministic machining processes such as single point diamond turning and milling.

Huang et al. [10] investigated the effect of rotational speed of the wheel on the ground surface quality in grinding silicon nitride through a series of experiments and they found that the surface quality (ductile mode) is improved with increasing rotational speed of the wheel. However, for surface generation (brittle mode), it is insignificantly affected by the variations of the rotational speed of the wheel and the wheel spindle vibration caused by the wheel imbalance limits the improvement of the ground surface quality. Zhang et al. [11] investigated the different surface generation mechanisms both for WC/Co and RB-SiC and found that phase boundary cracking is the dominate mode, but for WC/Co, plastic deformation and grain dislodgement are the primary mechanisms governing the surface generation. Kwak [12] used Taguchi parametric optimization approach to evaluate the effects of process parameters and grain size on geometric errors of the workpiece. It was found that the depth of cut is the dominant factor to determine the geometric error. Allor et al. [13] investigated the effects of abrasive sizes and concentration in grinding and they found that the size of abrasive grain and the speed of grinding wheel are significant factors affecting the surface roughness. Oliveira et al. [14] studied dressing variables, such as dressing depth, dressing velocity and geometry of the dressing tool which can affect

the surface topography generation of the grinding wheel. It was found that the wheel pattern produced by dressing can improve the machined surface roughness.

For theoretical analysis of surface generation in grinding, Ohbuchi and Obikawa [15] proposed a model of surface generation by considering the upheaval and residual volumetric material removal resulting from different grain shapes and cutting speeds. Agarwal and Rao [16] developed an analytical model to predict the surface roughness based on the statistical characteristics of the distribution of the abrasive grain and protrusion heights. Warnecke and Zitt [17] established a synthetic 3D model by considering the macro profile of the grinding wheel and micro grain geometry combining with grinding kinematics to describe the process of the generation of surface topography. Cao et al. [18] established a model by combining the relative micro-vibration between the grinding tool and the workpiece with the micro-interacting behavior of the active grains to determine the impact of the vibration amplitude, grit size and process parameters on surface generation in grinding. Actually, grinding marks caused by wheel vibration severely deteriorate accuracy and quality of the workpiece being ground, which are difficult to be removed by subsequent polishing process [19-21]. How to control and suppress the grinding marks is becoming a critical issue to optimize the grinding operation. Therefore, a theoretical model should be developed to describe the formation of surface patterns under various grinding conditions. It was found that the vibration caused by unbalanced wheel is the primary source results in grinding marks in ultra-precision grinding [22-24]. Chen et al. [25] analyzed the influence of the micro-vibration of the grinding wheel on the surface quality of the workpiece generated in ultra-precision grinding and they established a mathematical model for describing the error of the surface profile of the workpiece caused by the vibration with a presumed simple sinusoidal signal. Kuriyagawa et.al.[26] developed 2D model to analyse the relationship between the grinding marks and grinding conditions. It is found that concentric circle patterns and spiral marks involved in the nano-topography generation. For the concentric circle pattern, it results from the revolution speed variation of grinding wheel or workpiece. For spiral pattern, it is caused by the wheel unbalance, which is quite difficult to eliminate. In order to control and reduce the nano-topography caused by the grinding marks, Yoshihara et.al. [27] developed a 2D model to describe the amplitudes of cross sectional profile under different speed ratio between wheel rotation frequency and workpiece rotation frequency and spatial frequency analyses is adopted to verify the simulation results. However, the surface topography of the workpiece is affected by many more factors. There is a lack of comprehensive study of possible elements involved in the surface generation in ultra-precision grinding and the surface generation mechanism is still not well understood.

In order to gain insight into the surface generation in ultra-precision grinding and the effect of grinding variables on the ground surface, the Taguchi method is firstly employed to evaluate the relative effect of the machining parameters, and then single factor experiments are carried out to investigate the correlation among each grinding parameter on the surface generation. Hence, a theoretical model for predicting the regular spiral patterns is built and verified by experiments. Different mechanisms of material removal that contribute to surface generation are also investigated.

2. Experimental details

In ultra-precision grinding, material is removed by a combination of the fast rotating grinding wheel, a fine feed speed, very small depth of cut and slow spindle speed for the workpiece. The ground surface is generated by the continuous movement of the tool edge profile along the traverse direction (ignoring the abrasive grains). As shown in Figure 1, high-speed spinning grinding wheel (V_2) and the workpiece spindle speed V_1 together with a fine feed speed (V_f) under tiny depth of cut (H) can produce path interference in adjacent passes of the wheel, which is responsible for the surface generation. Operational parameters can decide the radial locus of the grinding wheel to cut the workpiece and can influence the surface roughness and surface topographies of the workpiece. It is clear that the tool cutting parameters, wheel geometry and relative displacement between the tool and the workpiece have a significant influence on surface generation. The maximum peak-to-valley height of an ideal ground profile R_t can be calculated as [28]

$$R_t = r - \sqrt{r^2 - \frac{S^2}{4}} = r\left(1 - \sqrt{1 - \frac{S^2}{4r^2}}\right) \tag{1}$$

Due to $S << r$

$$R_t = \frac{S^2}{8r} = \frac{V_f{}^2}{8rV_1^2} \tag{2}$$

Where r is the grinding wheel nose radius, S is the wheel traverse distance when the workpiece completes one revolution, which is in mm/rev, V_f is the tool feed speed in mm/min, V_1 is the workpiece rotation speed in r/min.

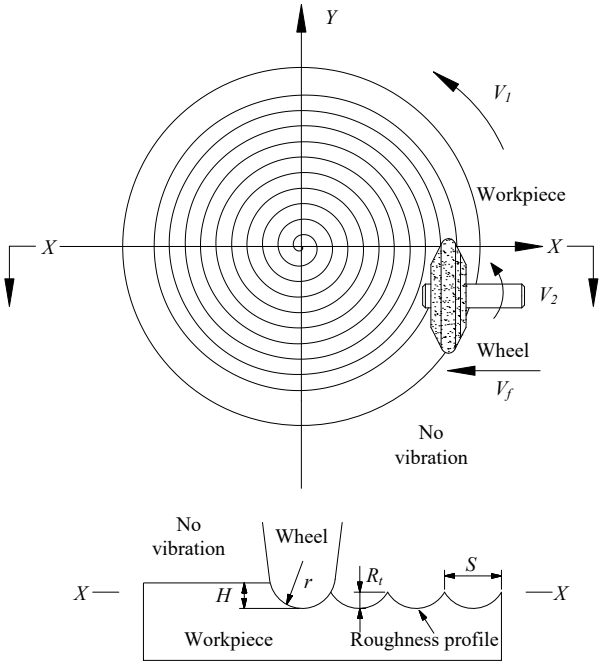

Figure 1 Surface generation in ultra-precision grinding

In the present study, ultra-precision grinding experiments were performed on a Moore Nanotech 450UPL ultra-precision grinding machine, which has two rotating spindles for the grinding wheel holder and the workpiece. The wheel holder is installed on a rotary B axis and the workpiece holder can be moved along the X axis, as shown in Figure. 2. In the experiments, a resin bonded diamond wheel with a grain size number of 500 is used and reaction bonded Silicon Carbide (RB-SiC) is selected for grinding material. The experimental conditions and material properties of RB-SiC are summarized in Table 1 and Table 2 respectively.

The major error sources and uncertainties originate from the random nature of the grinding wheel. In order to minimize the disturbance of the random errors, the spindle rotational speed of the grinding wheel is kept stable setting at 40000 rpm in the Taguchi experiments and in the single factor tests.

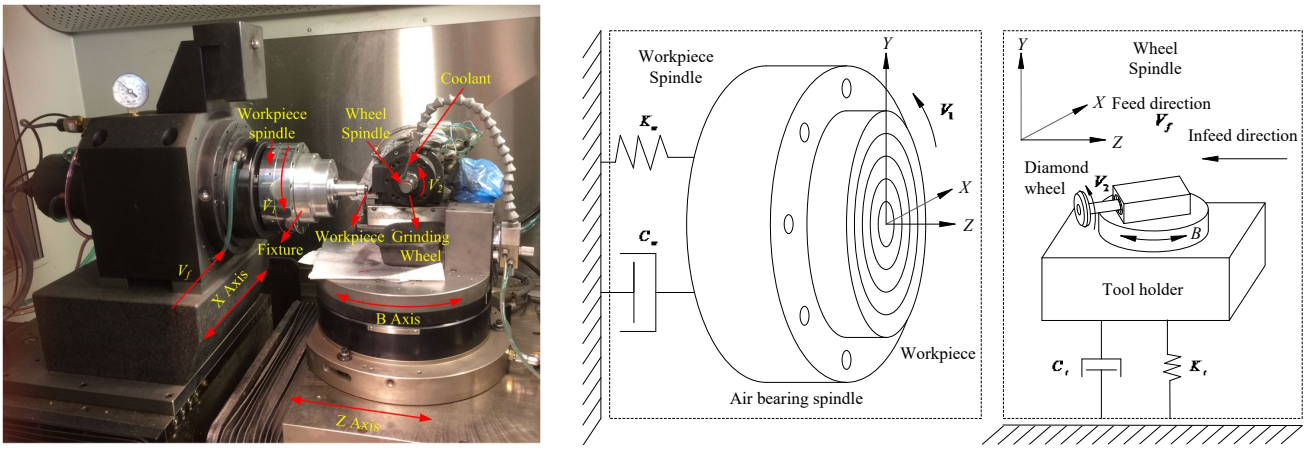

Figure 2 Schematic diagram of the grinding machine

The Taguchi approach is an engineering optimization method which is used to evaluate the influence of

process parameters or variables on process or product quality. It is able to optimize the machining parameters effectively with a minimum number of trials. To obtain a high performance in grinding RB-SiC, the combination of the grinding parameters is designed based on the Taguchi approach to evaluate the contribution of the process parameters (workpiece spindle rotational speed V_1, depth of cut H and feed speed V_f) with three levels on the arithmetical mean deviation of the profile (Ra). As shown in Table 3, the Taguchi method adopts the design of an orthogonal array, in which the three grinding factors are arranged in a L9 (3^3) orthogonal array. The grinding parameters are varied including the spindle speed of workpiece (V_1) in the range 500 rpm to 1500 rpm, the depth of cut (H) varied from 5 μm to 15 μm and the feed speed (V_f) in the range of 5 mm/min to 15 mm/min. Finally, the experimental results are converted into a signal-to-noise (S/N) ratio which is used to measure surface quality.

Table 1 Grinding wheel and grinding parameters

Grinding Wheel	Resin bonded diamond wheel: 500-grit , diameter: 18mm, thickness: 5mm, nose radius: 0.5 mm, Concentration 100%, Structural number 7
Speed of the grinding wheel (V_2) (rpm)	40000
Speed of the workpiece (V_1)(rpm)	500,1000,1500
Feed rate (V_f) (mm per min)	5,10,15
Depth of cut (μm)	5,10,15
Dresser and Truer	Single diamond nib and aluminium oxide stick
Coolant	CLAIRSOL 330

Table 2 Material properties of RB-SiC

Workpiece	Reaction Bonded SiC
Compressive strength (MPa)	2000
Young's modulus (H) (GPa)	410
Vickers hardness (H_v) (GPa)	2500
Fracture toughness (K_{IC})(MPa·m½)	4.0
Density(g/cm^3)	3.1
Dimension(Length × width × height)	9mm × 9 mm × 5mm

Table 3 Taguchi experimental design

No	Control factors	levels		
		1	2	3
A	V_1 (rpm)	500	1000	1500
B	H (μm)	5	10	15
C	V_f (mm/min)	5	10	15

3 Experimental results and theoretical analysis

3.1 Parametric analysis of surface generation

The measurement of the surface roughness of the workpiece was conducted by the non-contact Zygo Laser Interferometer Profiler System.The arithmetic roughness of the profile (Ra) is shown in Table 4. Figure 3 shows the value of the S/N ratios of three grinding parameters on the Ra value in different levels. In these experiments,

the smaller-the-better optmization criterion was adopted for the average S/N ratio and the larger value for the ratio infers better surface finish as shown in Table 5. It indicates that the feed speed (V_f) is a dominant varible for surface roughness and followed by spindle speed of the workpiece (V_1). The depth of cut (H) has insignificant effect on surface roughness. In Figure 3, it indicates that the optimal combination of grinding operation parameters is A3B2C1 (V_1=1500 rpm, H=10μm, V_f=5 mm/min).

Table 4 Experimental results for *Ra*

Experiment No.	Control factors			
	A	B	C	$Ra(\mu m)$
1	1	1	1	0.148
2	1	2	2	0.180
3	1	3	3	0.214
4	2	1	2	0.184
5	2	2	3	0.194
6	2	3	1	0.133
7	3	1	3	0.164
8	3	2	1	0.099
9	3	3	2	0.182

Table 5 S/N ratio factor response for *Ra*

Technical Parameters	Lever			Δ	Rank
	1	2	3		
A	14.96	15.49	16.86	1.90	2
B	15.67	16.41	15.24	1.17	3
C	18.07	14.80	14.45	3.62	1

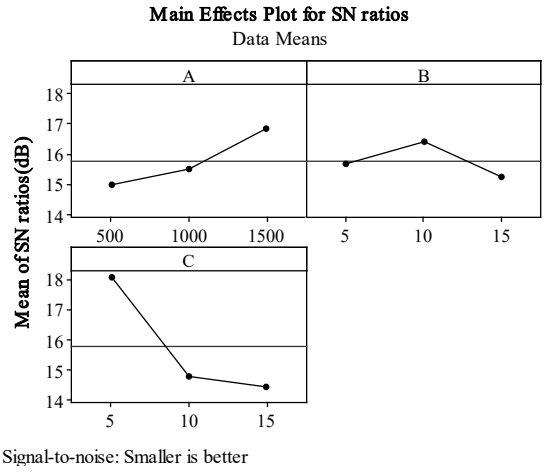

Figure 3 S/N ratio graph for the surface roughness *Ra*

Figure 4 shows the surface topographies of the ground RB-SiC surfaces. It is found that the most significant feature of the machined surfaces is the spiral marks around the rotational center of the workpiece, which does not correspond to that of the ideal surface as shown in Figure 1, without micro-vibration. Furthermore, the number of spirals is equal to the ratio of the rotational speed of the grinding wheel V_2 to the spindle speed of workpiece

V_1, e.g. spirals in Figure 4 (a) to 4 (c), the number of the spiral marks is equal to 80 (V_2 / V_1=40000/500=80) in one circle. The ratio space is much larger than the distance the tool travels and the shape of spiral marks varies as grinding parameters are varied, indicating that the tool vibration involved in surface generation in ultra-precision grinding. It is indicated that the vibration of the grinding wheel at the tool rotational frequency has a dominant impact on the evolution of surface generation. It is observed that the spirals density decrease with the increase of workpiece rotation speed (from $V_1 = 500$ rpm to 1000 rpm) when the speed ratio is an integer, which is related to the fact that the number of spirals is equal the ratio, as shown in Figure 4 (a) to 4 (f). However, when the ratio is not an integer (V_2 / V_1=40000/1500≈26.67), the spiral density appears a sharp increase, as shown in Figure 4 (g) to 4 (i). In this case, a phase shift (i,e. the fractional part of the ratio) generates an angle increment when the workpiece rotates one revolution. which indicates an accumulation of phase shift in the grinding cycles.

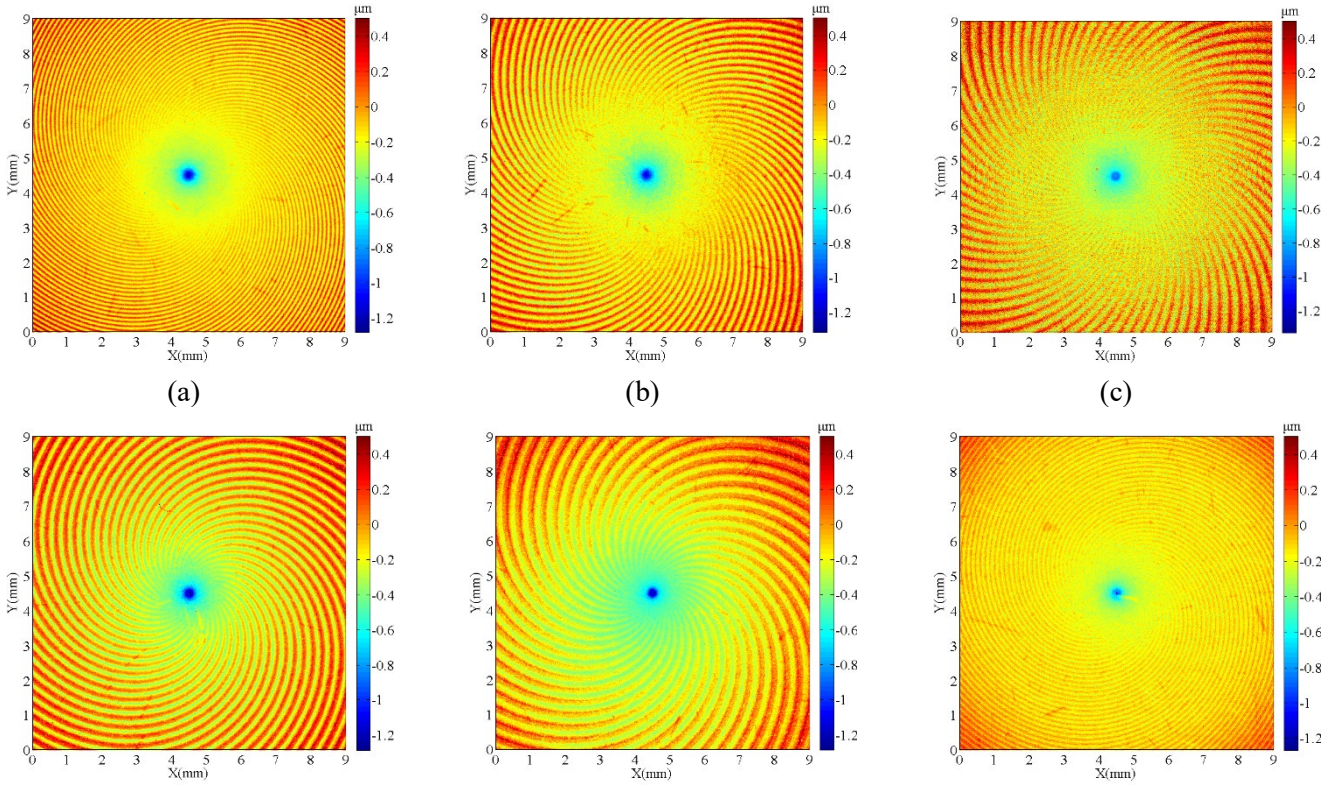

(a) (b) (c)

(d) (e) (f)

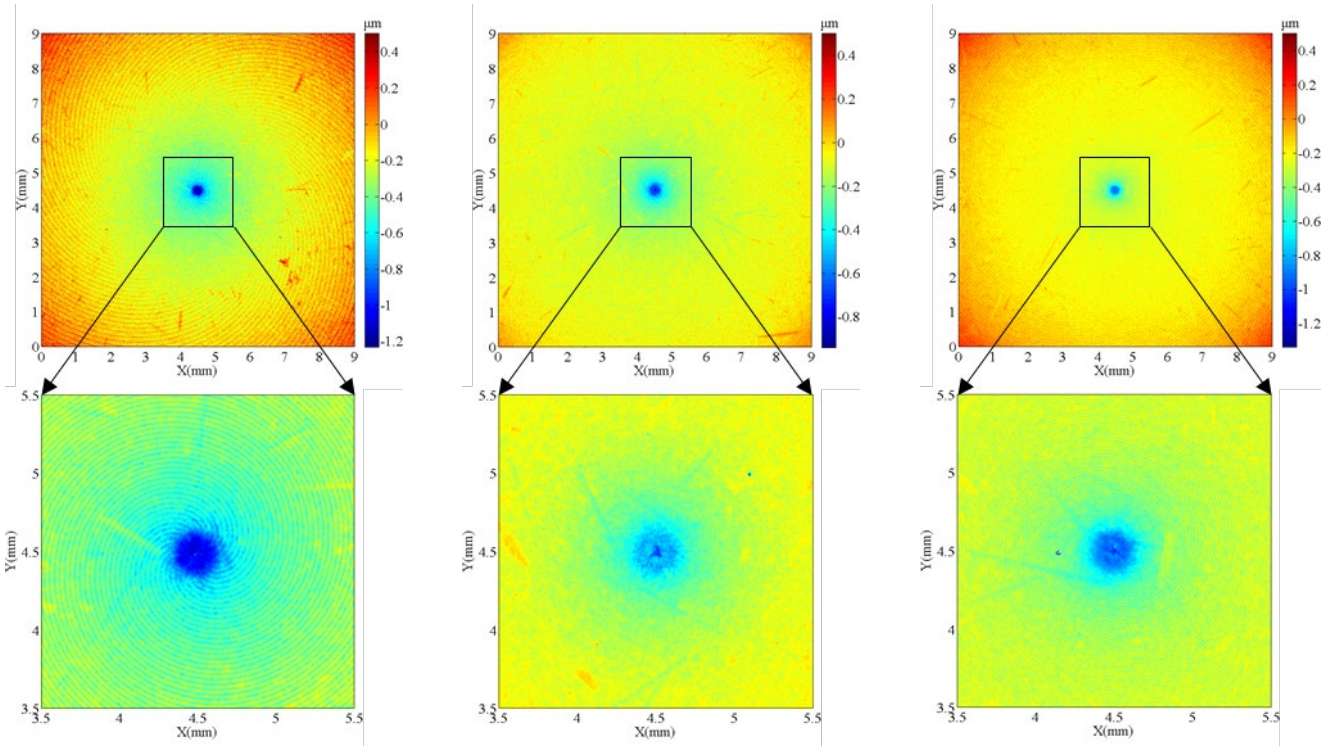

(g) (h) (i)

Figure 4 Contour map for surface topography determined in the Taguchi experiment

Based on the optimal result of the Taguchi experiments, a single-factor experiment is conducted to evaluate the effect of each machining parameter (i.e. workpiece rotational speed V_1, depth of cut H and feed speed V_f) on the surface quality. The effect of the process parameters on the surface roughness is shown in Figure 5. It is found that the surface roughness increases with increasing feed speed from 5 mm/min to 15 mm/min. The smaller feed speed results in the aggravation of the interference of the cutting profile of the wheel which leads to higher surface quality. The surface roughness decreases with increasing depth of cut from 5 μm to 10 μm. From 10 μm to 15 μm, the surface roughness slightly increases and the change in surface roughness is very tiny, which agrees well with the result of the Taguchi experiments. As the rotational speed of the workpiece increases, the surface roughness decreases, which is caused the decrease of cross-feed distance (V_f / V_1). The cross-feed distance represents the distance that the grinding wheel moves towards the workpiece center when the workpiece completes each revolution, which can increase neighbouring cutting profile interference resulting in a good surface finish. In Figure 5(d), for the same cross-feed distance, the average value of the surface roughness is used. With the increase of the cross-feed distance, the surface roughness increases. It shows that the cross-feed distance is also an important variable affecting the surface quality of the workpiece, which can reduce the scallop-height significantly so as to obtain good surface finish.

Table 6 Single-factor experimental results

No.	V_1	H	V_f	V_f / V_1	$Ra(\mu m)$
1	1500	10	5	0.003	0.082
2	1500	10	10	0.007	0.133
3	1500	10	15	0.010	0.236
4	1500	5	5	0.003	0.078
5	1500	10	5	0.003	0.073
6	1500	15	5	0.003	0.080
7	500	10	5	0.010	0.176
8	1000	10	5	0.005	0.121
9	1500	10	5	0.003	0.070

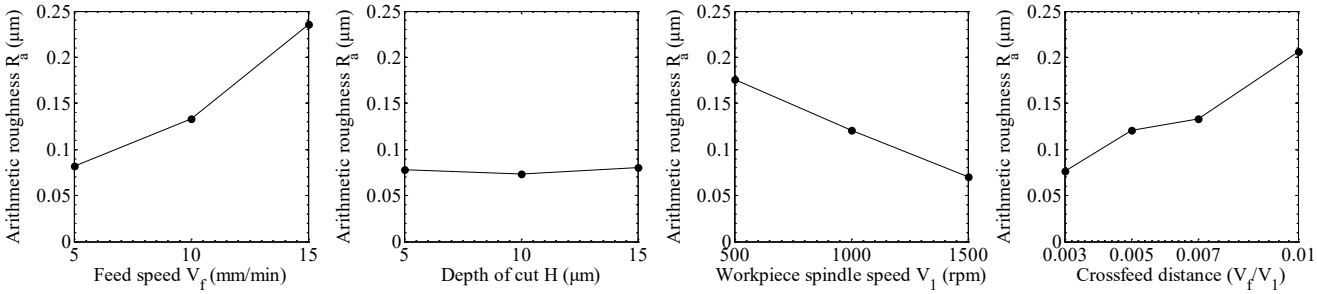

Figure 5 Effect of processing parameters on surface roughness in grinding RB-SiC

In order to investigate the effect of phase shift on surface generation in grinding, different phase shifts (0, 0.1…1.0) for different workpiece spindle speeds ($V_1 = 500$ rpm, $V_1 = 1000$ rpm and $V_1 = 1500$ rpm) are used. The rotational speed of the grinding wheel is increased starting at $V_2 = 39000$ rpm in a 50 rpm,100 rpm and 150 rpm intervals respectively until the two rotational speeds ratio (V_2 / V_1) is an integer again. Figure 6 shows the influence of phase shift on arithmetic surface roughness (S_a), it is interesting to note that all three curves embrace the similar tendency, as the phase shift increases from 0 to 0.1, the surface quality improves significantly although the variation of three rotational speed is very small. With the continuous increase of the phase shift to 0.6, the surface roughness is found to keep on improving. However, the surface quality becomes worse afterward with an increase of the phase shift from 0.6 to 1.0. It infers that the phase shift has a prominent effect on the surface finish of the ground surface. In order to obtain a better surface finish in grinding, the middle phase shift is preferable.

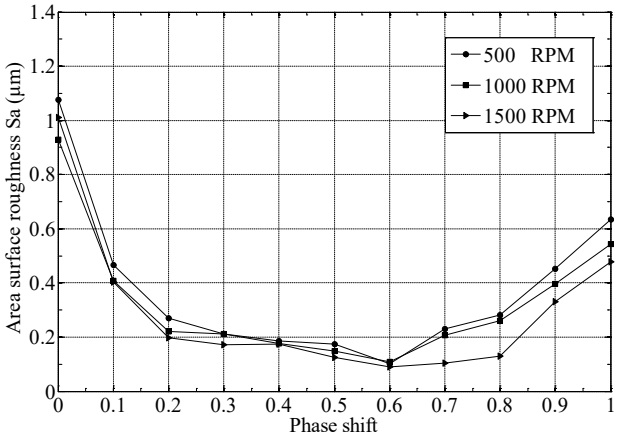

Figure 6 Influence of phase shift on surface roughness

3.2 Theoretical analysis of the surface generation

A theoretical model is purposely built to analyse the surface generation in ultra-precision grinding. The spiral masks have significant effect on surface quality, which have a strong correlation with the ratio of the rotational frequency of the grinding wheel to the workpiece. Figure 7 shows the mechanism of the generation of the spiral masks in the grinding process. After the workpiece rotates one revolution, the crossfeed distance the grinding wheel travelling the workpiece (direction of feed) is $S = V_f / V_1$. In an ideal condition with an integer ratio, the spirals marks have the same rotation angle as the previous tool masks without phase shift, which indicates the contour lines are straight lines instead of spirals. For a non-integer ratio, the fractional part of the ratio generates an increment Φ in phase shift when the workpiece rotates one revolution, which is responsible for the evolution of the spiral masks. In actual grinding operation, the phase shift always exists in the entire process due to the fluctuation of rotational frequency of the grinding wheel or the workpiece. The locus of the grinding wheel is shown in Figure 8.

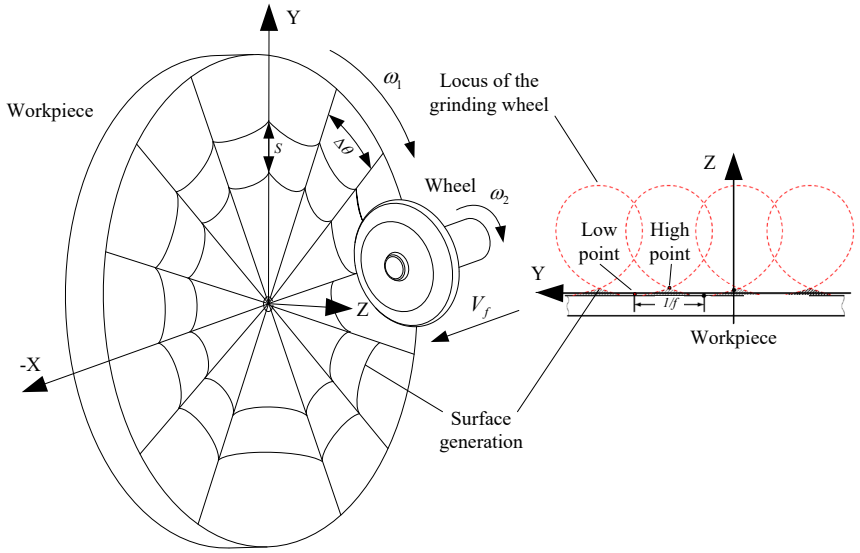

Figure 7 Spiral marks generated by the wheel with micro-vibration

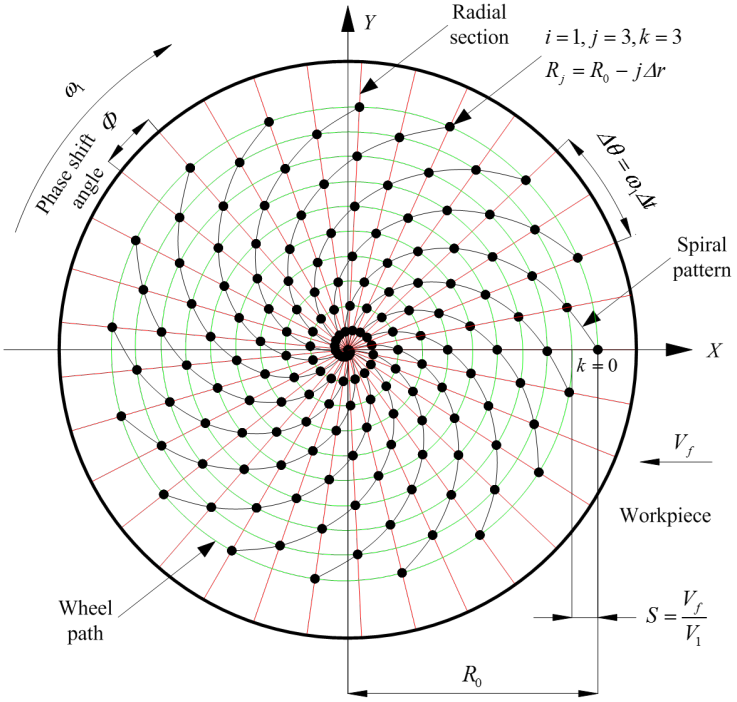

Figure 8 Locus of the lowest point for the grinding wheel

The workpiece rotates an angle $\Delta\theta$ when the grinding wheel completes one revolution Δt, which can be express as:

$$\Delta t = \frac{60}{V_2} \tag{3}$$

$$\Delta\theta = \frac{2\pi V_1}{V_2} \tag{4}$$

In the grinding, the number of spiral marks is equal to the integer part of rotating ratio of wheel and workpiece. The phase shift Φ represents fraction part of the rotating ratio, which can be calculated as:

$$\Phi = 2\pi\left[\frac{V_2}{V_1} - int\left(\frac{V_2}{V_1}\right)\right] \tag{5}$$

In discrete form, the harmonic motion of the grinding wheel can be expressed as:

$$Z(t_j) = A\sin(\frac{2\pi f_2 j\Delta\theta}{\omega_2} + \varphi),\quad j = 0,1,2,...,N_t \quad N_t = \frac{2\pi}{\omega_1\Delta t}\cdot\frac{R_0V_1}{V_f} \tag{6}$$

Where f_2 is the rotational frequency of the grinding wheel, A is the vibration amplitude.

$$\theta(i,k) = k\Delta\theta + 2\pi(i-1),\quad i = 1,2,...,N_w \quad N_w = \frac{R_0V_1}{V_f}, k = 0,1,2,...,N_s \quad N_s = \frac{2\pi}{\omega_1\Delta t} \tag{7}$$

$$R(i,k) = R_0 - \left[k + (i-1)N_s\right]\Delta r \quad \Delta r = \frac{V_f}{V_2} \tag{8}$$

In the $X-Y$ plane, the locus of the grinding wheel is given by:

$$X(i,k) = R(i,k)\cos\left[k\Delta\theta + 2\pi(i-1)\right] \tag{9}$$

$$Y(i,k) = R(i,k)\sin\left[k\Delta\theta + 2\pi(i-1)\right] \tag{10}$$

In order to investigate the relationship between the phase shift and spiral geometry, the single spiral simulation is conducted, in which the deepest point of interaction between the wheel and workpiece is considered. A simulation tool has been developed to implement model analysis of the surface generation in ultra-precision grinding by Matlab programming software. In ultra-precision grinding, the grinding wheel can not maintain complete invariability, instead there is a small revolution error which means that the phase shift is inevitable. It is found that the actual rotational speed of the wheel is about 20 rpm larger than the preset value. Figure 9 shows simulated results of the single spiral generation for different phase shifts (0, 0.1…1.0) through change the rotational speed of the grinding wheel from 39000 rpm to 40500 rpm in a 150 rpm intervals. It is found that with the increase of the phase shift (0-0.4), the cycles of spiral increase. When the phase shift is equal to 0.4, 0.5 and 0.6 the number of cycles keeps equal, after that the number decreases. At the same time the direction of rotation of spiral from anticlockwise to clockwise from the edge area to the centre area. Figure 10 shows the maps of grinding marks measured with the Zygo laser interferometric profiler. Due to the dense spiral marks as the accumulation of the phase shift, the small area (length×width=2mm×2mm) in the certre region of the workpiece is selected to make the spiral clearer to observe when the phase shift changes from 0.2 to 0.8, as shown in Figure 10 (c) to 10 (i). It can be observed that the test results agreed well with simulated spiral marks shown in Figure

9.

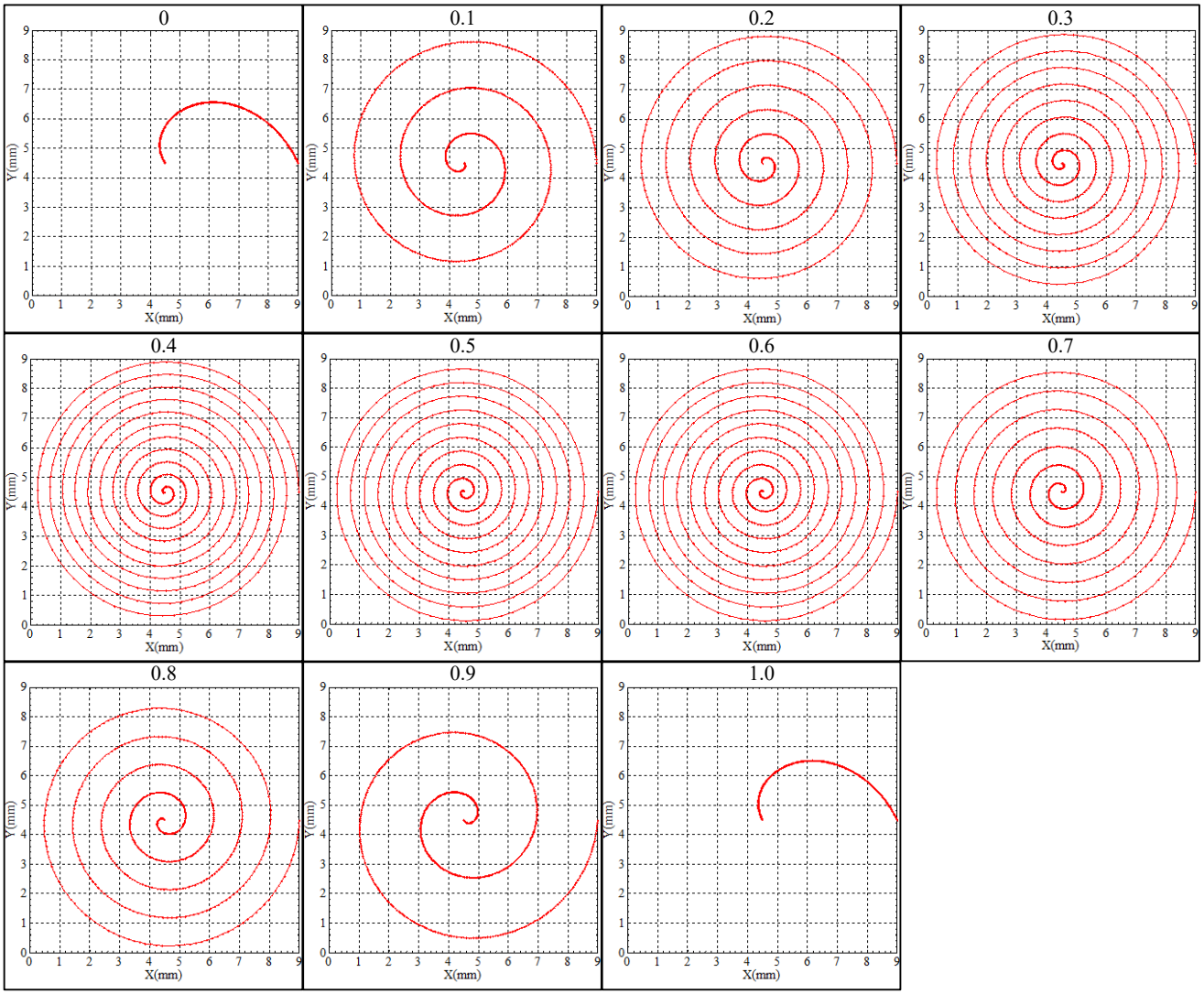

Figure 9 Simulation of single spiral generation (phase shift 0, 0.1…1.0), rotational speed of the grinding wheel: 39000-40500 rpm, feed rate: 10 mm/min, rotational speed of the workpiece 1500 rpm

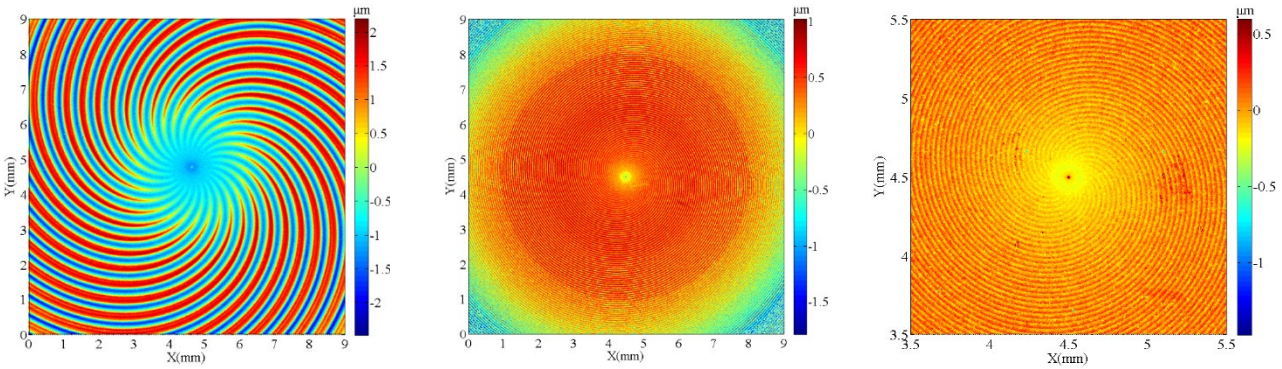

(a) (b) (c)

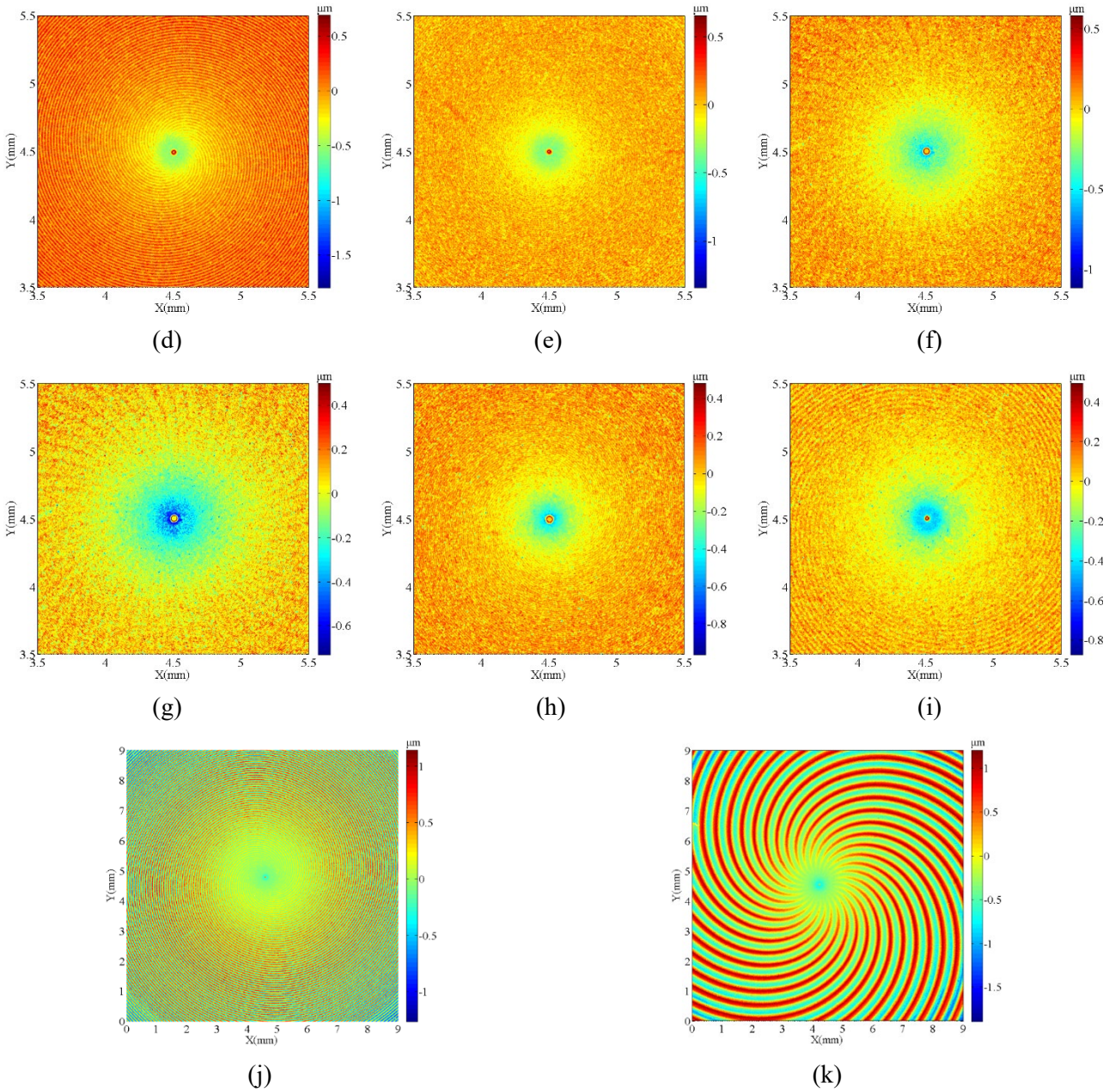

Figure 10 Measured surface topography for different phase shift (phase shift: 0, 0.1…1.0).The wheel speed V_2 from 39000 rpm to 40500 rpm in a 150 rpm intervals (V_1=1500 rpm, V_f=10 mm/min, H=10 μm)

The modelling of the surface pattern shown above gives the interaction between the wheel and workpiece without considering the variations of the feed rate. In fact, in the spark out stage, the feed speed is decreased gradually from the set value to 0 and the tool is then withdrawn and stopped. As a result, the area near the center is different from the rest of ground surface.

The position of the grinding wheel with respect to the workpiece can be amended as:

$$X_p(i,k) = (R_e - V_f \frac{\Delta\theta}{\omega_1} - a\frac{\Delta\theta^2}{2\omega_1^2})\cos\left[k\Delta\theta + 2\pi(i-1)\right] \tag{11}$$

$$Y_p(i,k) = (R_e - V_f \frac{\Delta\theta}{\omega_1} - a\frac{\Delta\theta^2}{2\omega_1^2})\sin\left[k\Delta\theta + 2\pi(i-1)\right] \tag{12}$$

R_e is the distance between the starting position of the wheel slowed for feed speed on the workpiece and the center of rotation of the workpiece.

$a < 0$ is the acceleration of feed speed near the central area.

With the development of wheel wear under micro vibration, more than one high point on the wheel surface may have opportunity to make contact with the workpiece [29]. Figure 11 shows two high points on the grinding wheel interact with the workpiece, and thus the number of waviness marks is doubled.

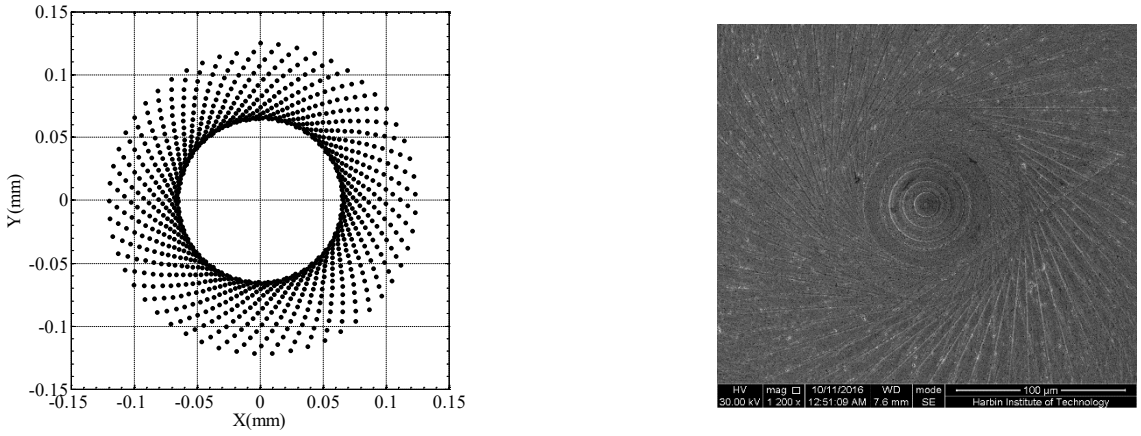

(a) (b)

Figure 11 The centre area (a) simulated surface pattern, (b) SEM map of ground surface (V_1=1500 rpm, V_2 =40000 rpm, V_f =10 mm/min, H =10 μm)

In order to calculate surface topography in each radical section, the shape of the wheel should be determined firstly. The grinding wheel profile having the wheel radius (R_w) and a nose radius (r_w) is modelled as an ellipsoid as shown in Figure 12, which can be expressed as

$$\left(\frac{x}{R_w}\right)^2 + \left(\frac{y}{R_y}\right)^2 + \left(\frac{z}{R_w}\right)^2 = 1 \tag{13}$$

where R_w and R_y are the semi-major axis and the semi-minor axis of the ellipse respectively.

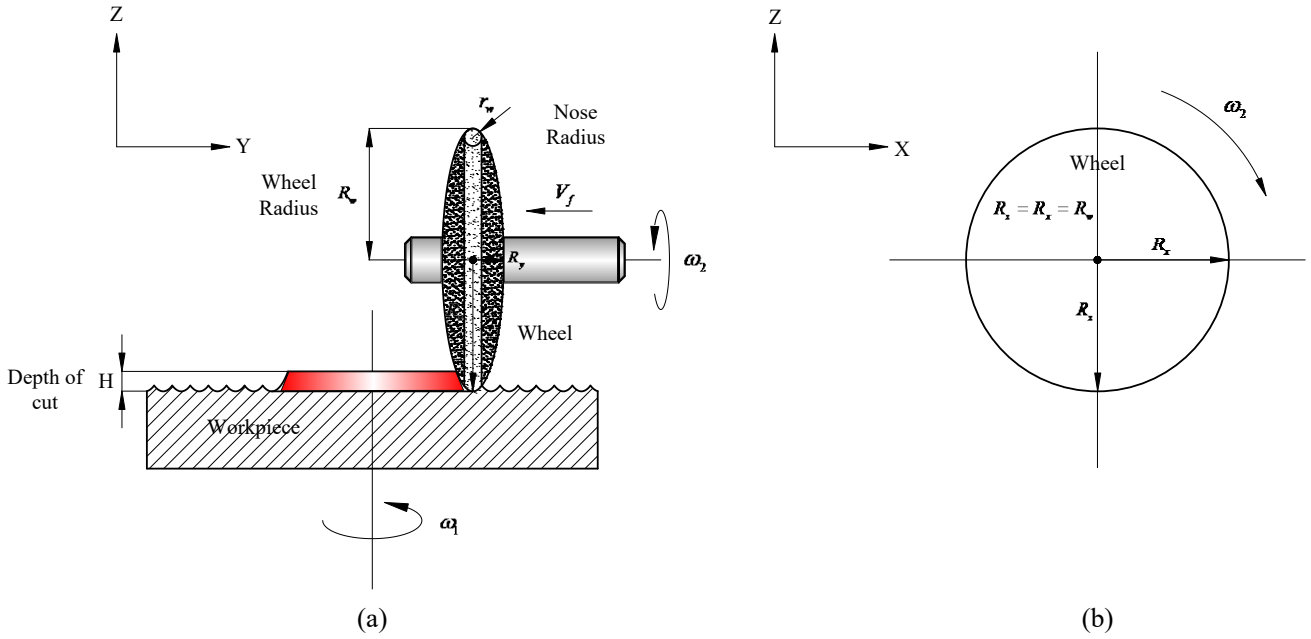

Figure 12 Graphical illustration of the grinding wheel: (a) Front view of the wheel (b) Side view of the wheel

In order to calculate (R_y), the radius of curvature (r_w') in $Z-Y$ section is derived as:

$$r_w' = \frac{1}{\rho} = \frac{\left[1+\left(\frac{\partial z}{\partial y}\right)^2\right]^{\frac{3}{2}}}{\left|\frac{\partial^2 z}{\partial y^2}\right|} \tag{14}$$

$$r_w' = \frac{1}{\rho} = \frac{\left[1+\frac{y^2 R_w^{\,2}}{R_y^{\,4}}\left(1-\frac{y^2}{R_y^{\,2}}\right)^{-1}\right]^{\frac{3}{2}}}{\left|\frac{R_w}{R_y^{\,2}}\left(1-\frac{y^2}{R_y^{\,2}}\right)^{-\frac{1}{2}}\left(1-\frac{y}{R_y^{\,2}}\left(1-\frac{y^2}{R_y^{\,2}}\right)^{-1}\right)\right|} \tag{15}$$

At the lowest contact point ($y=0$), the tool nose radius of the wheel is given as:

$$\frac{1}{\rho} = \frac{R_y^{\,2}}{R_w} = r_w \tag{16}$$

$$R_y = \sqrt{R_w r_w} \tag{17}$$

The final ellipsoid equation is denoted as:

$$\frac{x^2+z^2}{R_w{}^2}+\frac{y^2}{R_w r_w}=1 \tag{18}$$

To drive the intersection of neighbouring cutting profile, cross section of the grinding wheel in Z-Y plane can be expressed as :

$$z=-\sqrt{R_w{}^2-\frac{R_w y^2}{r_w}} \tag{19}$$

In discrete form

$$Z_{i,k}(r_{i,k})=-\sqrt{R_w{}^2-\frac{R_w\left[r_{i,k}-(i-1)S\right]^2}{r_w}} \tag{20}$$

The cutting profile for $i\,th$ and $i+1\,th$ at the $k\,th$ radical section can be expressed as

$$Z_c(r_{i,k})=A\sin\left\{\frac{2\pi f_2[k+(i-1)N_s]\Delta\theta}{\omega_2}+(i-1)\Phi\right\}+Z_{i,k}(r_{i,k}) \tag{21}$$

$$Z_c(r_{i+1,k})=A\sin\left[\frac{2\pi f_2(k+iN_s)\Delta\theta}{\omega_2}+i\Phi\right]+Z_{i+1,k}(r_{i+1,k}) \tag{22}$$

For the intersection of $i\,th$ and $i+1\,th$ cutting tool profile at the $k\,th$ radical section, $Z(R_{i,k})=Z(R_{i+1,k})$ and $r_{i,k}=r_{i+1,k}$. Thus, the height $Z_{i,i+1,k}$ of the intersection is determined as

$$Z_{i,i+1,k}=\frac{r_w}{2}(A_i+A_{i+1})-\sqrt{\frac{r_w(A_i+A_{i+1})^2+r_w(A_{i+1}-A_i)^2+R_wS^2}{4r}-\frac{R_wS^2(A_i-R_w{}^2)}{r_w(A_{i+1}-A_i)^2+R_wS^2}} \tag{23}$$

$$r_{i,i+1,k}=-\frac{2r_wZ_{i,i+1,k}(A_{i+1}-A_i)+r_w(A_{i+1}{}^2-A_i^2)+R_wS^2(1-2i)}{2R_wS} \tag{24}$$

where $A_i=A\sin\left\{\frac{2\pi f_2[k+(i-1)N_s]\Delta\theta}{\omega_2}+(i-1)\Phi\right\}$, $A_{i+1}=A\sin\left[\frac{2\pi f_2(k+iN_s)\Delta\theta}{\omega_2}+i\Phi\right]$

According to Eq 11 - Eq 24, all ground surface topographies in different radical sections can be calculated. Figure 13 shows the model agree with experiments in term of Sa under different phase shift ($V_1=1500$ rpm) in grinding of RB-SiC, in which the measured and calculation area are $X_L=Y_L=1\,mm$, and the centre of selected area $X_O=Y_O=3\,mm$ with respect to the centre of workpiece.

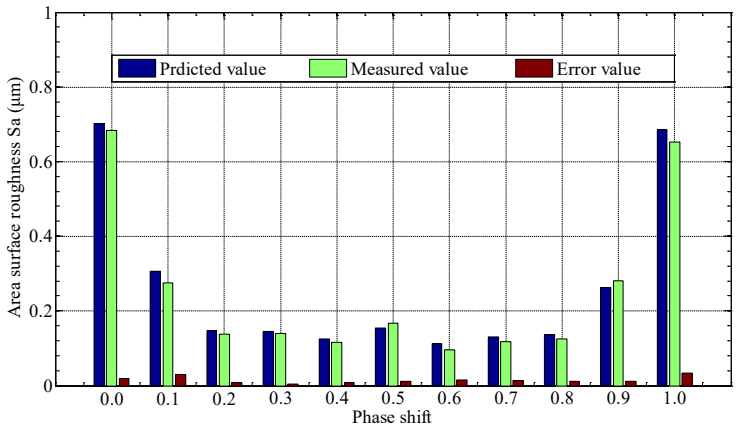

Figure 13 Comparison diagram between predicted and measured area surface roughness

Material properties play an important role in the process of chip formation and surface generation, expecially for the ceramics materials, which differs considerably from metals in grinding [30]. In order to study the different mechanisms of surface generation for different types of material, RB-SiC, mould steel (S136) and tungsten carbide (WC) are chosen for the grinding experiments. As shown in Figure 14, the spiral marks are observed on the ground surfaces of the three kinds of material, for steel and WC, the spirals are clearer to observe than that of RB-SiC, which resulted from more facture areas in comparison with steel and WC. The machined surfaces contain micro grooves produced by the micro cutting of the grinding wheel, especially for steel and WC, which are more clearly seen. For steel, the surface is generated by plastic flow, especially in the interaction between neighbouring cutting grooves, in which the later pass of the wheel extrudes the material aside. However, the machined surfaces for WC and RB-SiC are found to be more complex and contain micro fracture regions, pits and ductile areas. It is found that even some smooth regions are covered with smeared particles and fine debris, in which the material removed action is trapped between the wheel and workpiece in machining region. A few pits are observed on the machining surfaces of WC and RB-SiC. It is indicated that considerable differences existed in machining brittle materials and ductile metals, in which different modes of material removal would be involved in the surface generation. It is interesting to note that the Spanzipfel effect is found in grinding the three kinds of materials, in which a small portion of the materials is not removed by the cutting tool, instead it is left on the ground surface. The Spanzipfel effect is related to the minimum undeformed chip thickness, below which the chip can not be formed [31,32]. For steel, the Spanzipfel effect is more obvious than that of WC and RB-SiC.

*

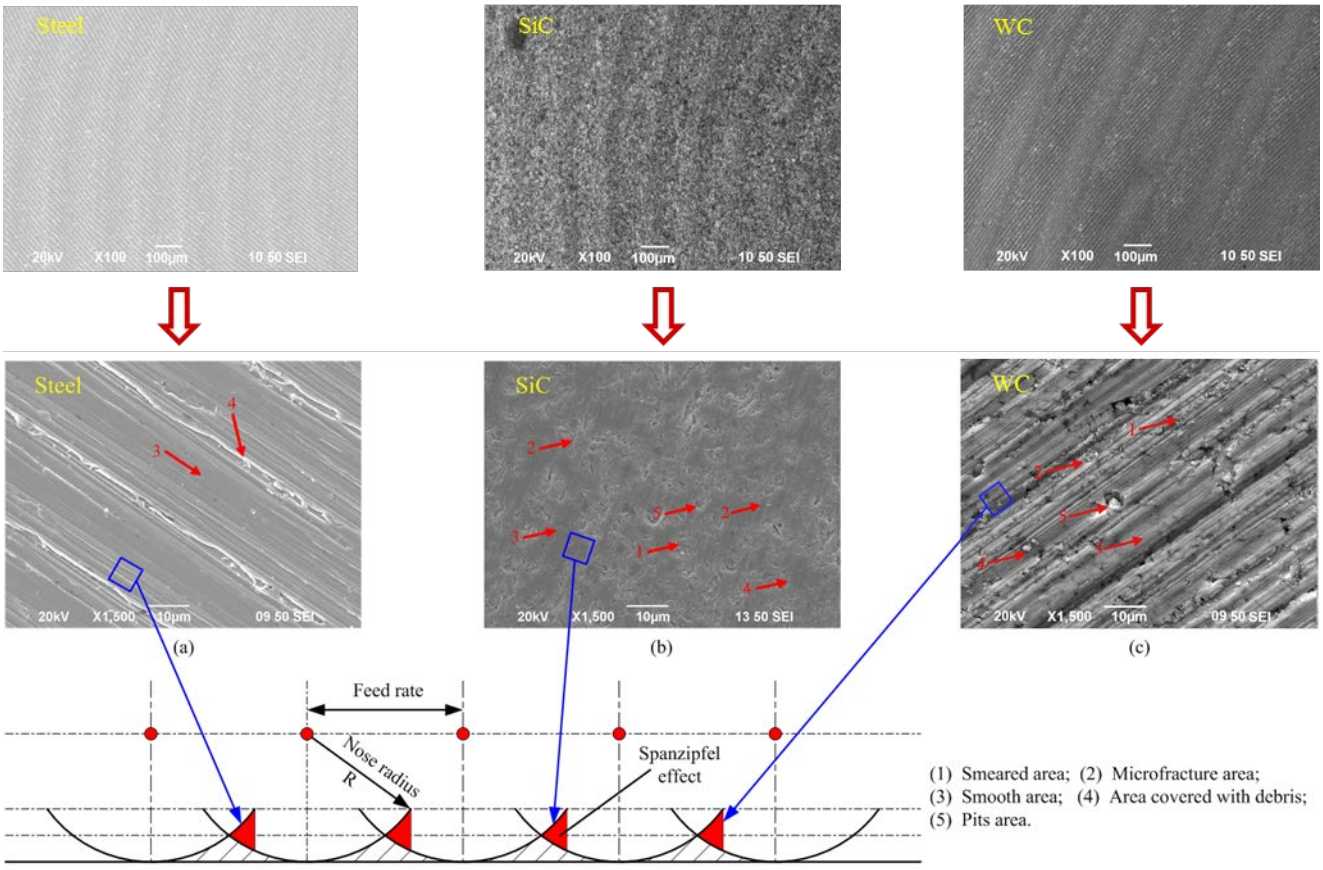

Figure 14 SEM micrographs of ground surface for (a) Steel, (b) RB-SiC and (c) WC (V_1=1500 rpm, V_2=40000 rpm, V_f=10 mm/min, H=10 μm). Arrows point at five typical areas: (1) smeared areas; (2) microfracture areas; (3) smooth areas; (4) area covered with debris; and (5) pits areas.

4 Conclusions

Surface generation in ultra-precision grinding has been systemically investigated both experimentally and theoretically. The ground surface quality is found to be primarily influenced by feed rate, workpiece spindle speed, synchronous vibration of the grinding wheel and phase shift. The optimal combination of the process parameters includes a small crossfeed distance and a finer feed rate as well as a medium phase shift. These factors can determine the trajectory of the grinding wheel and result in different surface topographies. A single spiral model model is developed to uncover the evolution of spiral marks. It is found that medium phase shift can result in dense spirals. The approximate straight line pattern around one circle is caused by the gradual decrease of the feed speed near the end of grinding operation. The surface generation in the grinding involves many mechanisms, such as spiral marks, Spanzipfel effect and phase shift. The Spanzipfel effect is found in grinding both for ductile materials and brittle materials.

Acknowledgments

The work was supported by a PhD studentship (project account code: RU3K) from The Hong Kong Polytechnic University. This research work was also supported by the State Key Basic Research and Development Program, China (973 program, Grant no. 2011CB 013202) and Guangdong Provincial Department of Science and Technology, Guangdong, P.R. China for The Introduction of Innovative R&D Team Program of Guangdong Province (Project no.:201001G0104781202).

References

1. Agarwal S, Rao PV (2012) Predictive modeling of undeformed chip thickness in ceramic grinding. International Journal of Machine Tools and Manufacture. 56:59–68
2. Beaucamp A, Simon P, Charlton P, King C, Matsubara A, Wegener K (2017) Brittle-ductile transition in shape adaptive grinding (SAG) of SiC aspheric optics. International Journal of Machine Tools and Manufacture 115: 29-37.
3. Jahanmir S, Ramulu M, Koshy P (1999) Machining of ceramics and composites. Marcel Dekker, New York
4. Zhang QL, To S, Zhao QL, Guo B, Zhang GQ (2015) Impact of material microstructure and diamond grit wear on surface finish in micro-grinding of RB-SiC/Si and WC/Co carbides. International Journal of Refractory Metals and Hard Materials 51:258-263
5. Agarwal S, Rao PV (2010) Grinding characteristics, material removal and damage formation mechanisms in high removal rate grinding of silicon carbide,International Journal of Machine Tools and Manufacture. 50:1077–1087
6. Yin L, Huang H (2008) Brittle materials in nano-abrasive fabrication of optical mirrorsurfaces. Precision Engineering 32:336–341
7. Zhang B, Zheng XL, Tokura H, Yoshikawa M (2003) Grinding induced damage in ceramics. Journal of Materials Processing Technology 132 (1-3):353-364
8. Lee SC, Ren N (1996) Behavior of elastic-plastic rough surface contacts as affected by surface topography, load, and material hardness. Tribology Transactions, 39(1), 67-74.
9. Stark GA, Moon KS (1999) Modeling surface texture in the peripheral milling process using neural

network, spline, and fractal methods with evidence of chaos. ASME Journal of Manufacturing Science and Engineering 121(2):251-256

10. Huang H, Yin L, Zhou LB (2003) High speed grinding of silicon nitride with resin bond diamond wheels, Journal of Materials Processing Technology 141(3):329-336
11. Zhang QL, To S, Zhao QL, Guo B (2016) Surface generation mechanism of WC/Co and RB-SiC/Si composites under high spindle speed grinding (HSSG). International Journal of Refractory Metals and Hard Materials 56:123-131
12. Kwak J (2005) Application of Taguchi and response surface methodologies for geometric error in surface grinding process. International Journal of Machine Tools and Manufacture 45(3):327-334
13. Allor RL, Whalen TJ, Baer JR, Kumar KV (1993) Machining of silicon nitride:experimental determination of process/property relationships. Proceedings of International Conference on Machining Advanced Materials 223–234
14. Oliveira JFG, Botteneand AC, França TV (2001) A novel dressing technique for texturing of ground surfaces. Annals of the CIRP—Manufacturing Technology 59:361–364
15. Ohbuchi Y, Obikawa T (2006) Surface generation model in grinding with effect of grain shape and cutting speed. JSME International Journal, Series C: Mechanical Systems Machine Elements and Manufacturing 49(1):114-120
16. Agarwal S, Rao PV (2005) A new surface roughness prediction model for ceramic grinding. Proceedings of the Institution of Mechanical Engineers, Part B: Journal of Engineering Manufacture 219(11):811-819
17. Warnecke G, Zitt U (1998) Kinematic simulation for analyzing and predicting high-performance grinding processes. Annals of the CIRP 47(1):265–270
18. Cao YL, Guan JY, Li B, Chen XL, Yang JG, Gan CB (2013) Modeling and simulation of grinding surface topography considering wheel vibration. The International Journal of Advanced Manufacturing Technology 66(5):937-945
19. Jiang XH, Guo MX, Li BZ (2018) Active control of high-frequency tool-workpiece vibration in micro-grinding. The International Journal of Advanced Manufacturing Technology 94(1):1429-1439
20. Yan Y, Xu J, Wiercigroch M (2016) Regenerative chatter in self-interrupted plunge grinding. Meccanica 51(12): 3185-3202
21. Hassui A, Diniz AE (2003) Correlating surface roughness and vibration on plunge cylindrical grinding of

steel. International Journal of Machine Tools and Manufacture 43(8):855-862

22. Yoshihara N, Kuriyagawa T, Syoji K (2003) Formation of vertical striped pattern on the ground surface in high-reciprocation profile grinding (in Japanese). Journal of the Japan Society for Precision Engineering 67(8):1316-1320
23. Cao HR, Dörgeloh T, Riemer O, Brinksmeier E (2017) Adaptive separation of unbalance vibration in air bearing spindles. Procedia CIRP 62:357-362
24. Marinescu I, Rowe W, Dimitrov B, Ohmori H (2013) Tribology of abrasive machining processes (2nd ed.). Amsterdam: Elsevier
25. Chen JB, Fang QH, Li P (2015) Effect of grinding wheel spindle vibration on surface roughness and subsurface damage in brittle material grinding. International Journal of Machine Tools and Manufacture 91:12-23
26. Kuriyagawa T, Yoshihara N, Saeki M, Syoji K (2003) Nano-topography characterization of axisymmetric aspherical ground surfaces. Key Engineering Materials 238-239:125-130
27. Yoshihara N, Yan JW, Kuriyagawa T (2008) Control of nano-topography on an axisymmetric ground surface. Key Engineering Materials 389-390:96-101
28. Whitehouse DJ (1994) Handbook of surface metrology. Bristol: Institute of Physics Pub.
29. Gill R (1986) An investigation into the effect of the ratio of grinding wheel speed to workpiece speed in the centreless grinding process. Coventry (Lanchester) Polytechnic, PhD thesis
30. Horvath M, Kundrak J, Mamalis A, Gyani K (2002) On the Precision Grinding of Advanced Ceramics. The International Journal of Advanced Manufacturing Technology 20(4):255-258
31. Pandit SM, Sathyanarayanan G (1984) Data-dependent systems approach to surface generation in grinding. ASME Journal of Engineering for Industry 106(3):205-212
32. Pandit SM, Revach SS (1981) A data dependent systems approach to dynamics of surface generation in turning. ASME Journal of Engineering for Industry 103(4):437-445